Available online at www.sciencedirect.com
ScienceDirect
Journal of Nuclear Materials 374 (2008) 109–115
journal of nuclear materials
www.elsevier.com/locate/jnucmat

Modelling precipitate distribution in reduced-activation steels

D. Gaude-Fugarolas *, Y. de Carlan

CEA Saclay, SRMA/La2M bât, 453, 91191 Gif Sur Yvette cedex, France

Received 27 March 2007; accepted 18 July 2007

Abstract

The microstructure and carbide distribution in two commercial creep resistant, low-activation, martensitic alloys (F82H and JLF-1) have been modelled using a thermo-kinetic calculation package. The microstructures after manufacturing and after long unstrained thermal aging treatments (13 500 h) at various temperatures (250, 400 and 550 °C), considered to be representative of service temperatures, have been considered. In all cases, the calculated carbide size distributions match in order of magnitude experimental measurements, although the shape of the distribution differs. The obtained results are more accurate for alloy F82H than for alloy JLF-1. Nevertheless, this work shows that it is possible to obtain realistic estimates of the microstructure evolution of creep resistant alloys in long thermal ageing treatments at service-like temperatures.

1. Introduction

Within the present international effort to develop a wide range of viable alternatives to fossil fuels, a special interest is being placed on the development of safer and more efficient nuclear power plants and on the use of fusion for power generation (ITER, DEMO). The process of selection of the best materials for each of the different parts of a power plant is one of the critical issues in its development. Moreover, many components need to be able to perform in very demanding conditions for all the planned life of the power plant without replacement. Therefore, a good understanding of their microstructure and mechanical behaviour during all their working life is indispensable. Obviously, it is not practical to perform life tests that last years before being able to select the material to use. It is therefore indispensable to put in place reliable modelling techniques that would allow to shorten the development time of such critical components.

F82H and JLF-1 are two of the reduced-activation ferritic/martensitic alloys that have been considered for various structural components (e.g. first wall and blanket structures) for DEMO [1,2]. In both cases they present good mechanical properties, adequate creep resistance up to 550 °C and limited radiological activation. Both alloys present a microstructure consisting of tempered martensite with precipitation reinforcement. The creep resistance, toughness and overall mechanical properties of these alloys depend directly on the stability of the reinforcing phases and their fine distribution. The work presented here shows how it is possible to describe and predict the distribution of those reinforcing phases in the *As Manufactured* material and during and after being annealed for 13 500 h at temperatures ranging from 250 to 550 °C (*Thermally Aged* condition), which are temperatures comparable to the ones found in service conditions. The calculated size and distribution of precipitates is compared the experimental data gathered experimentally using image analysis and transmission electron microscopy [3,4].

2. Materials and experimental procedures

Casts of F82H and JLF-1 steels were produced on an industrial scale ingots. The *As Manufactured* plates had been subjected to a normalising and tempering treatment [3,4], and supplied as 7.5 and 15 mm thick plates. The prior austenite grain size for F82H is 100 μm and for JLF-1

* Corresponding author.
E-mail address: dgaude@cantab.net (D. Gaude-Fugarolas).

0022-3115/$ - see front matter © 2007 Elsevier B.V. All rights reserved.
doi:10.1016/j.jnucmat.2007.07.013

Table 1
Nominal composition of the experimental alloys studied, in wt% [3,4]

Alloy	C	Si	Mn	Cr	V	W	N	Ta
F82H	0.087	0.10	0.21	7.46	0.15	1.96	0.0066	0.023
JLF-1	0.106	0.05	0.52	8.70	0.18	1.91	0.028	0.028

Table 2
Heat treatments considered, *As Manufactured* (normalisation and tempering) and *Thermally Aged* (normalisation, tempering and thermal aging) [3,4]

Alloy	Normalisation	Tempering	Thermal aging
F82H	0.6 h @ 1040 °C	1 h @ 750 °C	13 500 h @ 250, 400 and 550 °C
JLF-1	1 h @ 1050 °C	1 h @ 780 °C	13 500 h @ 250, 400 and 550 °C

25 μm [4]. The composition of each alloy is given in Table 1. The *As Manufactured* condition consisted in normalisation, quench and tempering. *Thermally aged* samples were annealed for 13 500 hours at three different temperatures: 250, 400 and 550 °C. These temperatures were specifically chosen for being representative of typical service conditions. Details of the heat treatments considered are summarised in Table 2.

3. Microstructural characterisation

Microstructure of both alloys in the different conditions studied had been characterised in a previous work by optical microscopy, SEM and TEM [3,4]. Prior austenite grain size had been determined following the procedure described by Barcelo and Brachet [5]. This method estimates the prior austenite grain size of samples of alloy F82H in 100 μm and of alloy JLF-1 in 25 μm [4]. The microstructure of both alloys consists in martensite laths decorated with various types of precipitates. F82H presents as well some regions where martensite has partially recrystalised during tempering to form equi-axed ferrite. Figs. 1 and 2 correspond to the characteristic microstructures of both alloys in the *As Manufactured* condition. In the first of them specially, the precipitate distribution suggests the prior austenite grain boundaries, and also shows the martensite lath structure.

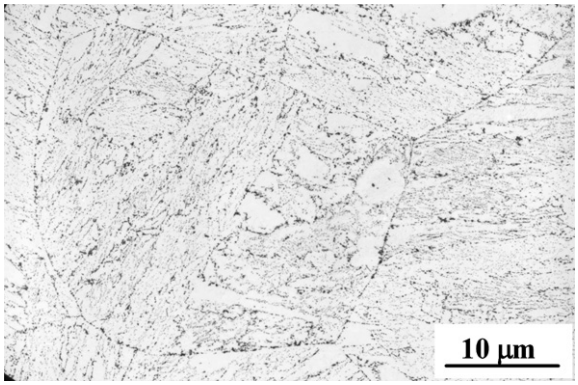

Fig. 1. Micrograph showing an overview of F82H precipitate distribution in the *As Manufactured* condition.

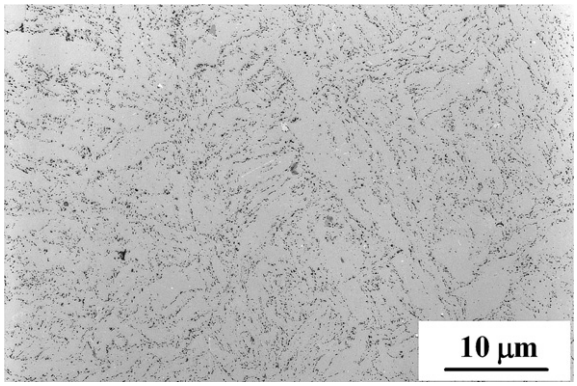

Fig. 2. Micrograph showing an overview of JLF-1 precipitate distribution in the *As Manufactured* condition.

Carbide extraction replicas were examined by TEM and image analysis used to determine the precipitate distribution. The experimental method to characterise the carbide distribution consisted in dissolving a thin layer of matrix, applying a carbon substrate to which the precipitates become adhered and then using image analysis on TEM micrographs of these carbon extraction replicas to determine the distribution. Rigourously, this type of methodology gives neither a 'surface distribution' nor a 'volume distribution' although if the thickness of the layer studied is taken into consideration, the measurement is an estimate of the volumetric distribution of precipitates. Even in such case, the performance of the extraction can be suspected to be a function of the size of the precipitate (i.e. a proportion of the precipitates much smaller than the thickness of the layer of matrix dissolved may be lost in the process and therefore, unaccounted for in the measurement) and different methods could be considered to try to correct that effect. In the experimental study used to validate the present calculations it was preferred to keep the measured distribution unadjusted [3,4]. The number of precipitates taken into account to determine the carbide distribution was just over 2000 precipitates per alloy and metallurgical condition on average (this value ranging from 1569 to 2671) [3].

The reinforcing phases are formed by a very fine and mostly stable distribution of MX precipitates and a distribution of coarser carbides. Larger carbides have been characterised as $M_{23}C_6$, but other carbides of varying stoichiometry and structure but similar morphology to $M_{23}C_6$ are present as well, specially in the case of JLF-1 steel [3,4]. The distribution of MX precipitates, once formed, remains stable during all treatments considered, with an average precipitate radius in the order of few nanometers.

After thermal aging, microstructure still consists of tempered martensite, and only the carbide distribution presents a noticeable evolution. Carbide composition varies slowly during thermal aging at all temperatures studied, and in

no case the occurrence of formation of Laves phases was observed [3,4].

4. Modelling precipitation

The simulation of the precipitation reactions has been performed using the theoretical model developed by Kozeschnik et al. at the Graz University of Technology [6–8]. This model is based on the thermodynamic extremum principle of maximum energy production, which in solid-state precipitation processes in equivalent to a constraint Gibbs free energy dissipation rate [9,10]. The model makes use of the CALPHAD-like thermodynamic database *IWS_Steel* also developed at the Graz University of Technology [6–8]. This model has been implemented in the software package MatCalc, of which the Linux implementation v.5.13/beta 16 has been used in the present work.

The *IWS_Steel* database, does not include the element tantalum. However, the database does include niobium which has a similar atomic structure to tantalum, and therefore it is reasonable to expected that for the aim of this work, it behaves in a sufficiently similar way. Therefore, an equivalent quantity of niobium has been used in the place of tantalum for the present calculations. Otherwise, the nominal composition of the alloys, as shown in Table 1 is the one that has been used in the calculations.

Matrix phases defined in the calculations are austenite and ferrite (martensite) as corresponds to thermodynamic criteria for each instant during the heat treatment. Dislocation densities for both phases have been taken from reference literature, with austenite presenting a dislocation density of 10^{11} m^{-2} and martensite 10^{14} m^{-2} [11,12]. Additional microstructural parameters used in the model have been taken from a previous work characterising the alloys [3,4]. Martensite laths have been described as being 0.1 μm thick and with an aspect ratio of 100 for F82H and 50 for JLF-1 [3]. Microstructural parameters are summarised in Table 3. For any additional microstructural parameters, the standard definition of each phase in MatCalc databases have been used.

Four types of precipitates have been included in the calculations, that is, cementite, M_7C_3, $M_{23}C_6$ and MX, which have been considered the essential phases required to describe the precipitation phenomena in the type of alloys considered. Each additional precipitation reaction adds substantially to the required computer resources needed to reach the completion of the calculation and for this reason, minor phases like M_4X_3 or M_6C, found only in alloy JLF-1 but not in F82H, have not been included in the calculations [3,4].

Finally, a choice about the precision of the calculation of the precipitate radius distribution needed to be made. During the calculations precipitates are considered as belonging to a number of *size classes* of particles with the same radius and composition. Individual size classes are created, rearranged and deleted during the calculation, allowing to model the evolution of the precipitate size distribution. Unfortunately, the choice of the number of classes represents a trade-off between calculation time and required precision. In order to assess the accuracy of the precipitate distribution, all calculations have been performed using an intermediate precision. A large precision (i.e. 250 size classes) would have yielded a more precise distribution, but it would have made the modelling of the thermal aging treatments excessively demanding computationally. Furthermore, it has been deemed more appropriate to use the same precision for all calculations. Therefore, both for the normalisation and tempering treatment and for the thermal aging treatments spanning thousands of hours, only 50 size classes have been used, which has still been able to produce an estimation of the size distribution, but permitting to complete the calculations within a reasonable amount of time.

Table 3
Microstructure parameters used in the calculations [3,4], and dislocation densities in each phase [11,12]

Alloy:	F82H	JLF-1		F82H	JLF-1
Austenite			Martensite		
Grain size/μm	100	25	Lath thickness/μm	0.1	0.1
			Lath aspect ratio	100	50
Dislocation density/m^{-2}	10^{11}	10^{11}		10^{14}	10^{14}

5. Results and discussion

5.1. General heat treatment

The thermo-kinetic model package MatCalc has been chosen for this work due to its capacity to calculate the evolution of the microstructure, especially the nucleation, growth and eventual coarsening or redissolution of the various types of precipitates in complex multi-component systems. The evolution of the precipitate phases considered during the tempering stage of the heat treatment leading to the *As Manufactured* condition) for alloy JLF-1 is shown in Figs. 3 and 4. Only the tempering stage has been plotted because all precipitate reactions start to occur during this stage.

The heat treatment simulated is described in Table 2. The evolution of the precipitation reactions can be seen in Fig. 3. In that Figure it is possible to appreciate that the normalisation temperature is sufficient to solubilise all elements, and that it is not until subsequent stages in the treatment that precipitation occurs. Full dissolution of all precipitates during normalisation is expected for this alloy composition although in alloys with higher nitrogen content it would be expected that higher normalisation temperature would be required to completely solubilise all MX precipitates.

During the tempering treatment, a classical sequence of precipitation occurs, starting with a brief appearance of cementite, which disappears swiftly with the precipitation

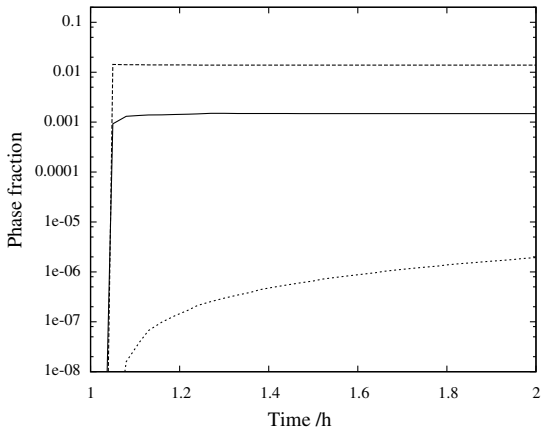

Fig. 3. Evolution of the precipitate phase percentage in alloy JLF-1 during the tempering stage of the *As Manufactured* treatment. Solid line corresponds to MX precipitates; dashed line to M_7C_3 and dotted line to $M_{23}C_6$.

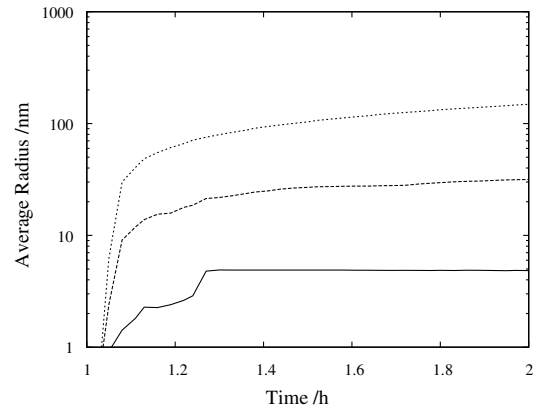

Fig. 4. Evolution of the precipitate average radius in alloy JLF-1 during the tempering stage of the *As Manufactured* treatment. Solid line corresponds to MX precipitates; dashed line to M_7C_3 and dotted line to $M_{23}C_6$.

of the more stable carbides M_7C_3 and $M_{23}C_6$ [13]. The most stable of the carbides considered is $M_{23}C_6$, although the kinetics of redissolution of M_7C_3 for alloys of the composition considered in this work are specially slow, specially at lower temperatures. Consequently is not altogether surprising to find that the carbide distribution is formed by a combination of various types of carbides, presenting a range of composition and size, although similar morphologies. In the present work only cementite, M_7C_3 and $M_{23}C_6$ have been considered.

Finally, Fig. 4 shows the evolution of the average radius for each of the precipitating phases MX, M_7C_3 and $M_{23}C_6$. This value takes into account all particles with radii above the critical stability radius for that precipitating phase.

From the later two Figures it is interesting to notice that, according to the simulation, for an alloy of composition of JLF-1 the carbide distribution is formed mainly by M_7C_3-type carbides of small size but also includes a smaller proportion of much larger $M_{23}C_6$-type carbides. These two carbides present similar morphologies, although they could, in principle, be easily differentiated from their composition. Actually, as the composition of precipitating carbides rarely matches the equilibrium composition for that phase [14], that is not straightforward, and it would be expected that what occurs is a continuous variation in composition as precipitates form and grow [13]. Once the carbide has formed, its composition tends towards its equilibrium composition. In any case, in the next section, when the carbide distribution calculated during this work is compared with the experimentally determined carbide distribution, both carbide distributions have been considered to be part of the one single carbide distribution.

5.2. Carbide distribution and evolution

The carbide distribution obtained in the calculations is compared with the distribution determined experimentally [3,4]. In all cases, it is expected that the profile of the calculated carbide distribution will be narrower than the one obtained from direct experimental measurements, due to the fact that the model considers a completely homogeneous material in terms of composition and microstructural description, while a real material will never show such homogeneity. The composition of the real alloy presents small variations around the nominal composition, and parameters like grain size or martensite lath thickness and dislocation density vary also locally. This develops in a distribution of precipitates that has seen contributions from all those different conditions. Obviously, although it would be possible to model that variability by considering the variance of all parameters involved, it would add substantially to the computer time required to obtain the calculation. On the other hand, it was expected that the mean value of carbide radius obtained from the calculation would be representative of the distribution found experimentally, and that the distribution would be acceptably accurate.

The average carbide radii determined experimentally are compared to the average carbide radii calculated in Table 4. For both alloys, the calculations describe correctly the

Table 4
Comparison of average carbide radii experimentally determined [3,4] and calculated

		Experimental $\bar{R}$/nm	σ/nm	Calculated $\bar{R}$/nm
F82H	AR	21	14	21
	250	24	15	21
	400	26	16	21
	550	25	15	26
JLF-1	AR	25	17	33
	250	25	14	32
	400	24	15	32
	550	22	14	35

AR stands for normalised and tempered condition, and 250, 400, 550 correspond to the thermal aging treatments at each of those temperatures. $\bar{R}$ is the average radius and σ the standard deviation of the experimental measurements.

stability of the carbide distribution, even after long thermal aging treatments. In the case of alloy JLF-1, the model overestimates consistently the average size of the carbide distribution, although stays in the correct order of magnitude both for the normalising and tempering treatment and for all long thermal annealing treatments.

The experimentally determined and calculated distributions are shown in Figs. 5–8 for alloy F82H and Figs. 9 and 10 for alloy JLF-1. The calculation proves to be able to give a good estimate of the order of magnitude of the mean carbide radius, although the determination of the precise shape of the distribution bell is less accurate. For instance, the bell of the theoretical distribution is narrower than the experimental one, but this would be expected due to a series of facts, due to shortcomings in both the model and on the experimental method used to determine the experimental precipitate distribution. On one hand, and as described above, the model considers one homogeneous composition and averaged microstructure, while the real materials present small inhomogeneities in both composition and microstructural parameters. The only way to model the mentioned inhomogeneities would involve producing a number of calculations covering a range of composition and microstructure and superimpose their results. Doing so, would produce a wider distribution of precipitates that would be closer to the one existent in the real material. However, it would increase substantially the computer time needed to reach the final result. On the other hand there the various sources of experimental error that on accumulation lead to a widening of the measured distribution with respect to the real precipitate population

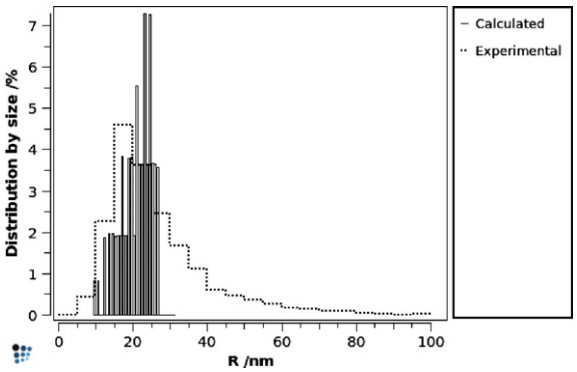

Fig. 5. Comparison between carbide distribution determined experimentally (dotted line) and calculated (bars) for alloy F82H in the *As Manufactured* condition.

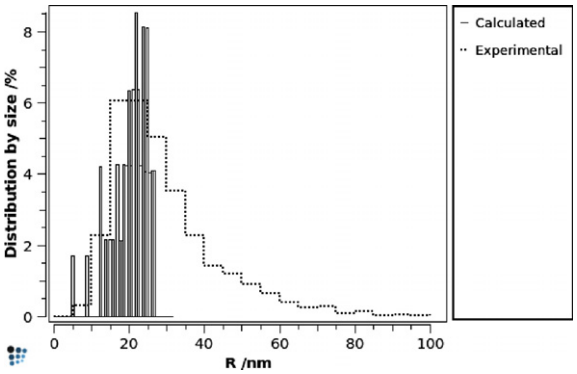

Fig. 6. Comparison between carbide distribution determined experimentally (dotted line) and calculated (bars) for alloy F82H after thermal aging at 250 °C.

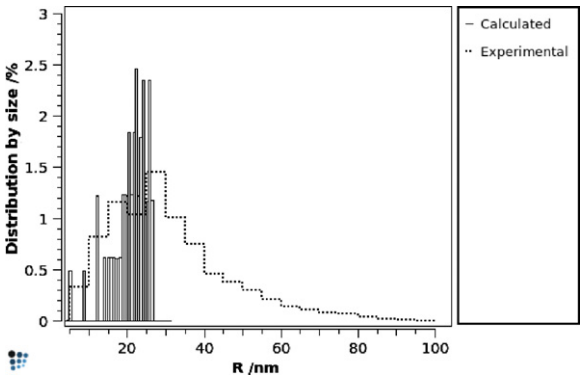

Fig. 7. Comparison between carbide distribution determined experimentally (dotted line) and calculated (bars) for alloy F82H after thermal aging at 400 °C.

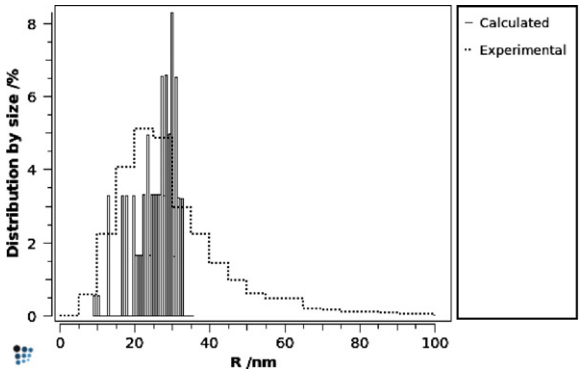

Fig. 8. Comparison between carbide distribution determined experimentally (dotted line) and calculated (bars) for alloy F82H after thermal aging at 550 °C.

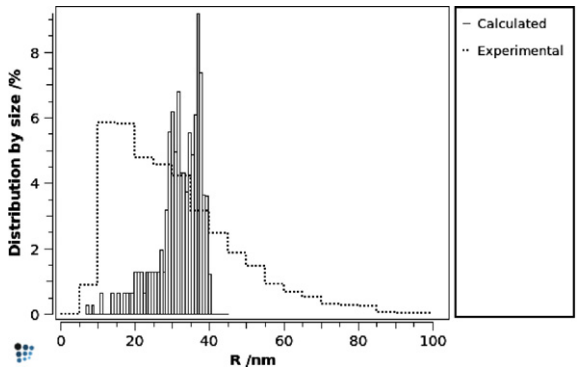

Fig. 9. Comparison between carbide distribution determined experimentally (dotted line) and calculated (bars) for alloy JLF-1 in the *As Manufactured* condition.

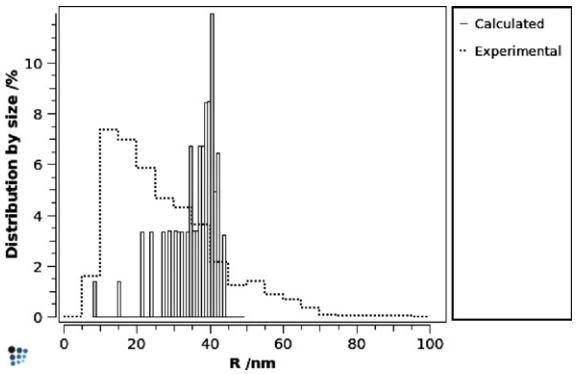

Fig. 10. Comparison between carbide distribution determined experimentally (dotted line) and calculated (bars) for alloy JLF-1 after thermal aging at 550 °C.

[15]. Two main sources of error are considered to affect the measurements by de Carlan and Alamo [3,4]. On one hand there is the measurement error due to the experimental method used in the determination of the carbide distribution (image analysis performed on micrographies of carbide extraction replica) that is difficult to eliminate altogether. On the other hand there is a possible statistical artifact due to the influence of the radius of the precipitate on the performance of carbide extraction. During the experimental characterisation of the precipitate distribution, it was assumed that the performance of the method was constant for all particle sizes [3,4].

As for the differences in accuracy for different alloys, it is clear that the calculations corresponding to alloy F82H (Figs. 5–8) are more precise than the ones for JLF-1 (Figs. 9 and 10), as it was already seen when comparing the average carbide radii in Table 4. In the later case, the model tends to consistently overestimate the average carbide radii, while still remaining within the correct order of magnitude. On the other hand, the samples of steel JLF-1 presented a more complex microstructure than F82H, with a more diverse range of precipitates [3,4], some of which have not been included in the calculation, and that could help explain the discrepancies between calculated and experimentally determined carbide distributions.

As a final reflection, it is the view of the authors that although it was not the aim of the study at this stage to deal with the effect of stresses on the evolution of the microstructure, nor the effect of irradiation, these aspects need to be the subject of continuation studies. The design of new alloys for high temperature applications requires to be able to model and describe the evolution of the microstructures of real, multi-component, multi-phase alloys during service conditions. Two elements are needed for that, on one hand, models that are able to describe the complex phenomena of microstructure evolution in real materials under creep conditions and under irradiation, and of course, suitable experimental data to be able to corroborate the validity of such predictions.

To that end, a package like the one used in this work has shown the capability to model the evolution of the microstructure under thermal ageing treatments, and therefore it would be interesting to apply its capabilities to look into some of the aspects related to microstructure evolution at high temperatures under stress and also under irradiation. Just to give one example of the aspects of the effect of irradiation damage in precipitation reactions that could be considered using the models used in the present work would be to look into the increase in diffusivity of some elements with the increase in vacancies, and the subsequent effect in the kinetics of precipitation.

6. Conclusion

The microstructure and carbide distribution in two commercial creep resistant, reduced-activation alloys (F82H and JLF-1) have been simulated using a thermo-kinetic model package. The microstructures after manufacturing and after long thermal aging treatments (13 500 h) at various temperatures, comparable to temperatures found during service conditions, have been considered.

In all cases, the calculated carbide distributions are a good estimate of the average carbide size found in experimental measurements. However, the results are more accurate for alloy F82H than for alloy JLF-1. Nevertheless, the results of the modelling show that it is possible to estimate accurately the evolution of the microstructure and carbide distribution even for extremely long heat treatments, at temperatures comparable to the ones found in real service conditions of power plant applications.

The present work shows that the microstructure evolution during long unstressed thermal aging treatments of multi-component, multi-phase alloys can be modelled accurately. The natural continuation of this work is to use the same models in the study of the effect of stresses on the evolution of the microstructure and on the kinetics of precipitation. These aspects need to be the subject of future studies, given that suitable experimental data becomes available.

References

[1] A.A.F. Tavassoli, J. Nucl. Mater. 302 (2002) 73.
[2] S. Jitsukawa, A. Kimura, A. Kohyama, R.L. Klueh, A.A. Tavassoli, B. van der Schaaf, G.R. Odette, J.W. Rensman, M. Victoria, C. Petersen, J. Nucl. Mater. 329–333 (2004) 39.
[3] Y. de Carlan, A. Alamo, Effects of Thermal Ageing on Microstructure and Mechanical Properties of 7.5/9cr (w/ta/v) Reduced-activation Martensitic Steels – Final Report Contract sm 2.1.1. Technical Report, CEA Saclay -SRMA, 1999.
[4] Y. de Carlan, A. Alamo, M.H. Mathon, G. Geoffroy, A. Castaign, J. Nucl. Mater. 283–287 (2000) 672.
[5] F. Barcelo, J.-C. Brachet, Quantification par analyse d'images de la taille de l'ancien grain austénitique d'aciers martensitiques 9Cr–1Mo. La Revue de Métallurgie – CIT Science et Génie des Matériaux, 1994, p. 255.
[6] J. Svoboda, F.D. Fischer, P. Fratzl, E. Kozeschnik, Mater. Sci. Eng. A A385 (2004) 166.
[7] E. Kozeschnik, J. Svoboda, P. Fratzl, F.D. Fischer, Mater. Sci. Eng. A A385 (2004) 157.

[8] E. Kozeschnik, J. Svoboda, F.D. Fischer, Comput. Coupl. Phase Diagrams Thermochem. 28 (2004) 379.
[9] L. Onsager, Phys. Rev. 37 (1931) 405.
[10] L. Onsager, Phys. Rev. 38 (1931) 2265.
[11] R.W. Hertzberg, Deformation and Fracture Mechanics of Engineering Materials, John Wiley & sons, Inc., New York, 1996.
[12] R.W.K. Honeycombe, H.K.D.H. Bhadeshia, Steels, Microstructure and Properties, 2nd Ed., Edward Arnold, London, 1995.
[13] H.K.D.H. Bhadeshia, In: 5th International Charles Parsons Turbine Conference, 2000, p. 3.
[14] J. Chance, N. Ridley, Metall. Trans. A 12 (1981) 1205–1213.
[15] A. Prat, X. Tort-Martorell, P. Grima, Estadística teórica y aplicada: entregas 1 a 4, C.P.D.A. – Universitat Politècnica de Catalunya, Barcelona, 1992.